Bulletin of the Seismological Society of America, Vol. 96, No. 5, pp. 1675–1688, October 2006, doi: 10.1785/0120050257

Homogeneity of Small-Scale Earthquake Faulting, Stress, and Fault Strength

by Jeanne L. Hardebeck

Abstract Small-scale faulting at seismogenic depths in the crust appears to be more homogeneous than previously thought. I study three new high-quality focal-mechanism datasets of small ($M < \sim 3$) earthquakes in southern California, the east San Francisco Bay, and the aftershock sequence of the 1989 Loma Prieta earthquake. I quantify the degree of mechanism variability on a range of length scales by comparing the hypocentral distance between every pair of events and the angular difference between their focal mechanisms. Closely spaced earthquakes (interhypocentral distance $<\sim 2$ km) tend to have very similar focal mechanisms, often identical to within the 1-sigma uncertainty of $\sim 25°$. This observed similarity implies that in small volumes of crust, while faults of many orientations may or may not be present, only similarly oriented fault planes produce earthquakes contemporaneously. On these short length scales, the crustal stress orientation and fault strength (coefficient of friction) are inferred to be homogeneous as well, to produce such similar earthquakes. Over larger length scales (~2–50 km), focal mechanisms become more diverse with increasing interhypocentral distance (differing on average by 40–70°). Mechanism variability on ~2- to 50-km length scales can be explained by relatively small variations (~30%) in stress or fault strength. It is possible that most of this small apparent heterogeneity in stress or strength comes from measurement error in the focal mechanisms, as negligible variation in stress or fault strength (<10%) is needed if each earthquake is assigned the optimally oriented focal mechanism within the 1-sigma confidence region. This local homogeneity in stress orientation and fault strength is encouraging, implying it may be possible to measure these parameters with enough precision to be useful in studying and modeling large earthquakes.

Introduction

Earthquake behavior is influenced by the strength and frictional properties of faults, and by the stresses in the Earth's crust. The degree of heterogeneity of fault strength and the degree of heterogeneity of crustal stress, and the length scales of these heterogeneities, have important implications for understanding and modeling earthquake physics. If stress and fault strength are relatively homogeneous on short length scales, then it may eventually be possible to accurately measure these parameters over the surfaces of particular faults. Knowing stress and fault strength would allow us to characterize the physics of a fault and to model important behaviors such as the response of the fault to a stress change or the rupture propagation of potential future earthquakes. However, if stress and/or fault strength are heterogeneous on short length scales it may be impossible to measure these parameters with adequate spatial resolution, and they would have to be modeled probabilistically.

Stress and fault strength, in general, are currently thought to be heterogeneous on short length scales. There are very few direct measurements of stress at seismogenic depths (~5–20 km), so the degree of heterogeneity has primarily been inferred from the variability of the fault orientations of nearby small earthquakes ($M < \sim 3$) (e.g., Hardebeck and Hauksson, 2001; Rivera and Kanamori, 2002). The observed focal-mechanism diversity has been interpreted to imply very complex small-scale fault structure, with fractures of a wide variety of orientations active contemporaneously in small volumes of crust. Small earthquakes are more difficult to observe than large ones, however, because of the lack of surface rupture or deformation, the greater attenuation of high-frequency seismic waves, and lower signal-to-noise ratios. Therefore, it is possible that part, or even all, of the apparent variability in the orientations of small earthquakes, and therefore the inferred stress and/or strength heterogeneity, comes from measurement error.

Here I investigate small-scale fault structure in California using high-quality small-earthquake datasets. The goals are to assess the variability of earthquake focal mechanisms on various length scales and to investigate the implications for heterogeneity or homogeneity of stress and fault strength. I explicitly consider the effect of uncertainty in earthquake locations and focal mechanisms on the apparent variability.

Data

The southern California earthquake catalog has been relocated using a 3D seismic velocity model (Hauksson, 2000) and source-specific station terms (SSST) (Richards-Dinger and Shearer, 2000), both of which account for the effects of 3D velocity structure in the crust. Waveform cross-correlation of the entire catalog has been used to significantly improve the relative locations of nearby events, through both double-difference relocation (hypoDD [Waldhauser and Ellsworth, 2000]) (Hauksson and Shearer, 2005) and relative relocation of similar event clusters (Shearer *et al.*, 2005). I compute focal mechanisms from Southern California Seismic Network (SCSN) *P*-wave polarities and *S*-wave/*P*-wave amplitude ratios measured from waveforms recorded at 140 three-component stations of the SCSN, Anza network, and portable instrument deployments. The focal mechanisms are computed using the method of Hardebeck and Shearer (2002, 2003), and uncertainty is estimated from the solution stability with respect to input parameter perturbations. High-quality solutions (Quality A and B of Hardebeck and Shearer [2002]) were found for 6380 earthquakes, mostly M 1.5–3.5, in southern California occurring during 1984–2003 (Fig. 1). I show later that the selection criteria for high-quality mechanisms do not bias the results. All of these location and focal mechanism catalogs are available from the Southern California Earthquake Data Center alternate catalogs web page (http://www.data.scec.org/research/altcatalogs.html).

I also study two areas of northern California, the aftershock region of the 1989 M_w 6.9 Loma Prieta earthquake and the East San Francisco Bay. I relocate earthquakes in these regions by using existing 3D seismic-velocity models (Eberhart-Phillips and Michael, 1998; Hardebeck *et al.*, 2004) and also double-difference (Waldhauser and Ellsworth, 2000). Because of the strong seismic-velocity contrasts across the Hayward and San Andreas faults, raytracing in the 3D seismic velocity models is performed to compute the take-off angles used for the focal mechanisms. *P*-wave polarities from the Northern California Seismic Network (NCSN) were used with the technique of Hardebeck and Shearer (2002) to find high-quality mechanisms for 1472 earthquakes from 1969 to 2004 in the East San Francisco Bay and for 496 aftershocks of the 1989 Loma Prieta earthquake (Fig. 1). Most events in these datasets are M 1–2.

Small-Scale Fault Structure

I study the degree of fault-orientation heterogeneity for small earthquakes by investigating the variability of the focal mechanisms on various length scales. For each of the three datasets, I consider every pair of events to find the spatial distance between them and the angular difference between their focal mechanisms. The angular difference is the minimum rotation about any axis to bring the two mechanisms into alignment. Hypocentral distance is measured using each of the available relocated catalogs. I then bin all of the event pairs by spatial distance and find the average angular difference for each bin (Fig. 2). This provides a measure of the mechanism variability at a range of length scales.

The closer events have more similar focal mechanisms, on average. The exact relationship between event distance and average focal-mechanism difference varies for the three datasets, but each shows a clear decrease in average mechanism difference for shorter hypocentral distances. Average mechanism difference decreases from ~60° for events >10 km apart, to ~40° for events ~1 km apart. On short length scales on the order of the relative location uncertainty, ~100 m, the average focal-mechanism difference reaches a minimum of 24°–32°. The average mechanism uncertainty is 26°, and even for a set of identical events, one would not expect the average mechanism difference to be significantly smaller than this. Therefore, it cannot be ruled out that the closest pairs of events, colocated to within the uncertainty, actually have identical focal mechanisms.

The focal-mechanism similarity of nearby events is also evident in histograms of the distribution of angular differences for each distance bin (Fig. 3). Distant pairs of events (>10 km apart) exhibit relatively uniform distributions of mechanism differences (the tapering at the high and low ends of the distributions is due to the smaller number of possible mechanism pairs in these ranges). In contrast, the histograms for very spatially close events (~100 m apart) are distinctly peaked at or below the average mechanism uncertainty, with many mechanism pairs identical to within the mechanism uncertainty. The transition takes place at an interhypocentral distance of ~500 m for the southern California dataset, on the order of the inferred dimensions of the earthquakes, implying that some of the small-scale structural homogeneity may be due to the instability of cross-cutting faults. However, the transition distance is ~2 km for the Loma Prieta data and ~5 km for the East Bay data, much larger than the earthquakes' dimensions.

I perform tests on synthetic data simulating the southern California dataset to demonstrate that the observed increased mechanism similarity for closely spaced events is not an artifact of any part of the analysis procedure. An example of a potential source of artifacts is the similarity in station distributions between nearby events, which might influence which types of mechanisms are best constrained and hence included in the high-quality datasets. Other artifacts may come from errors in the velocity model. Nearby events sample similar parts of the model and would be affected similarly by any errors, whereas more distant events sample different parts of the model which may introduce different errors.

For the synthetic tests, I use the same source and station locations as the real southern California dataset and assign "correct" focal mechanisms randomly either from the whole set of observed mechanisms or from a restricted subset. Polarity values are assigned to stations assuming that Hauksson's (2000) 3D velocity model is the "true" velocity structure, and a set of 1D velocity models are used in the

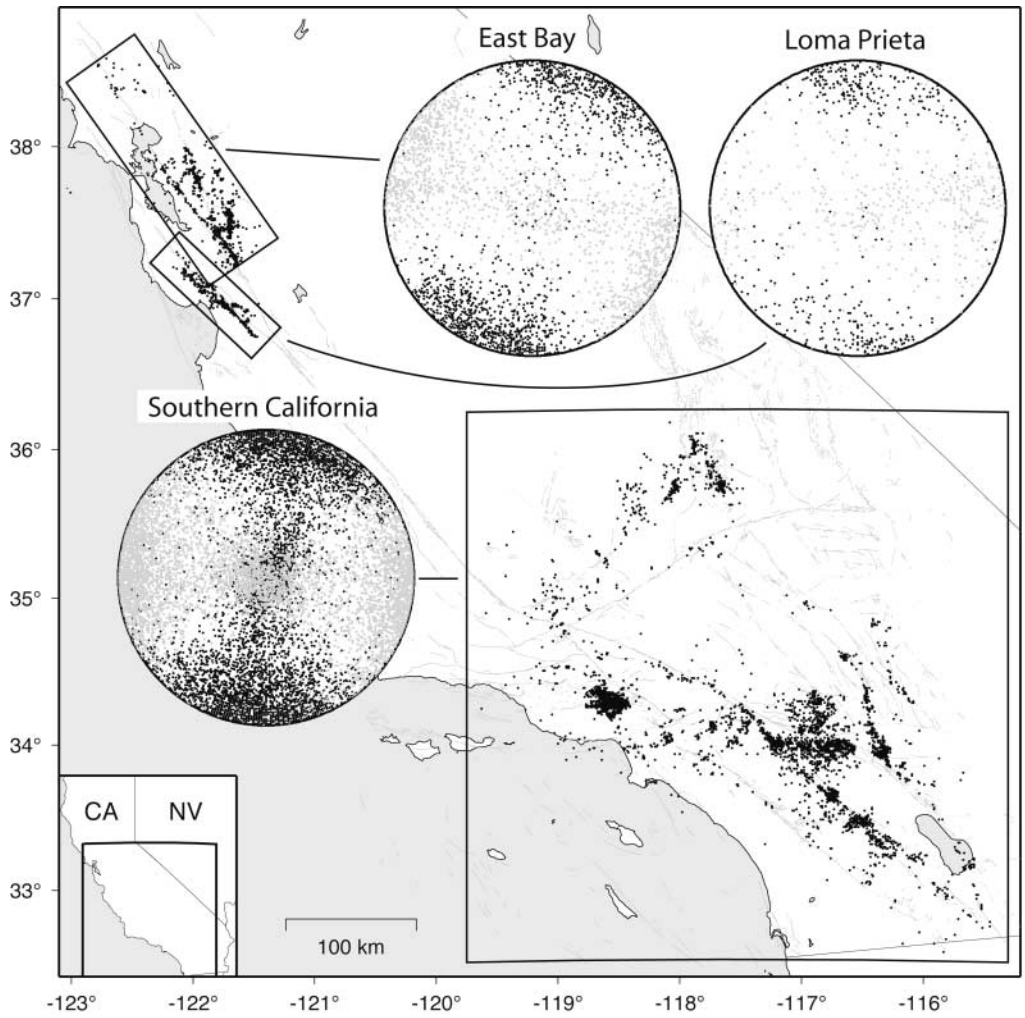

Figure 1. The spatial extent of the three California datasets is shown as boxes in map view, with the earthquake locations as black dots. The distribution of focal mechanisms in each dataset is represented by lower-hemisphere projections of the *P* axes (black dots) and *T* axes (grey dots). Focal mechanisms were found from *P*-wave first-motion polarities and *S*-wave/*P*-wave amplitude ratios (for southern California only), using the method of Hardebeck and Shearer (2002, 2003). The southern California dataset contains focal mechanisms for 6380 earthquakes from 1984 to 2003, the East San Francisco Bay dataset contains 1472 mechanisms for earthquakes from 1969 to 2004, and the Loma Prieta dataset contains mechanisms for 496 aftershocks from 1989 to 1993. Note that there are no events in the intersection of the East Bay and Loma Prieta datasets.

computation of the focal mechanisms, simulating the effects of unmodeled velocity structure. Measurement error is introduced by randomly reversing 10% of the synthetic polarity data and adding a 30% error to synthetic *S*/*P* amplitude ratios. Focal mechanisms are computed just as they were for the real dataset, and high-quality solutions are selected using the same criteria. Neither of the synthetic tests (Fig. 4) reproduces the observed increased mechanism similarity of nearby events. The synthetic dataset derived from diverse mechanisms shows a wide range of mechanism difference at all length scales, with many dissimilar nearby events. The synthetic dataset derived from a restricted set of similar mechanisms shows similar mechanisms at all length scales. Therefore, the observed increased mechanism similarity of nearby events does not appear to be an artifact of the focal-mechanism computations or the analysis.

The synthetic tests also provide an explanation for the long tails of the angular difference histograms at short interevent distances where the majority of mechanism pairs are very similar (e.g., Fig. 3). The distribution for a synthetic test with identical "correct" focal mechanisms (Fig. 5a) exhibits a long tail that is entirely the result of focal-mechanism measurement errors. Focal-mechanism errors are not normally distributed, as solutions can jump from one local min-

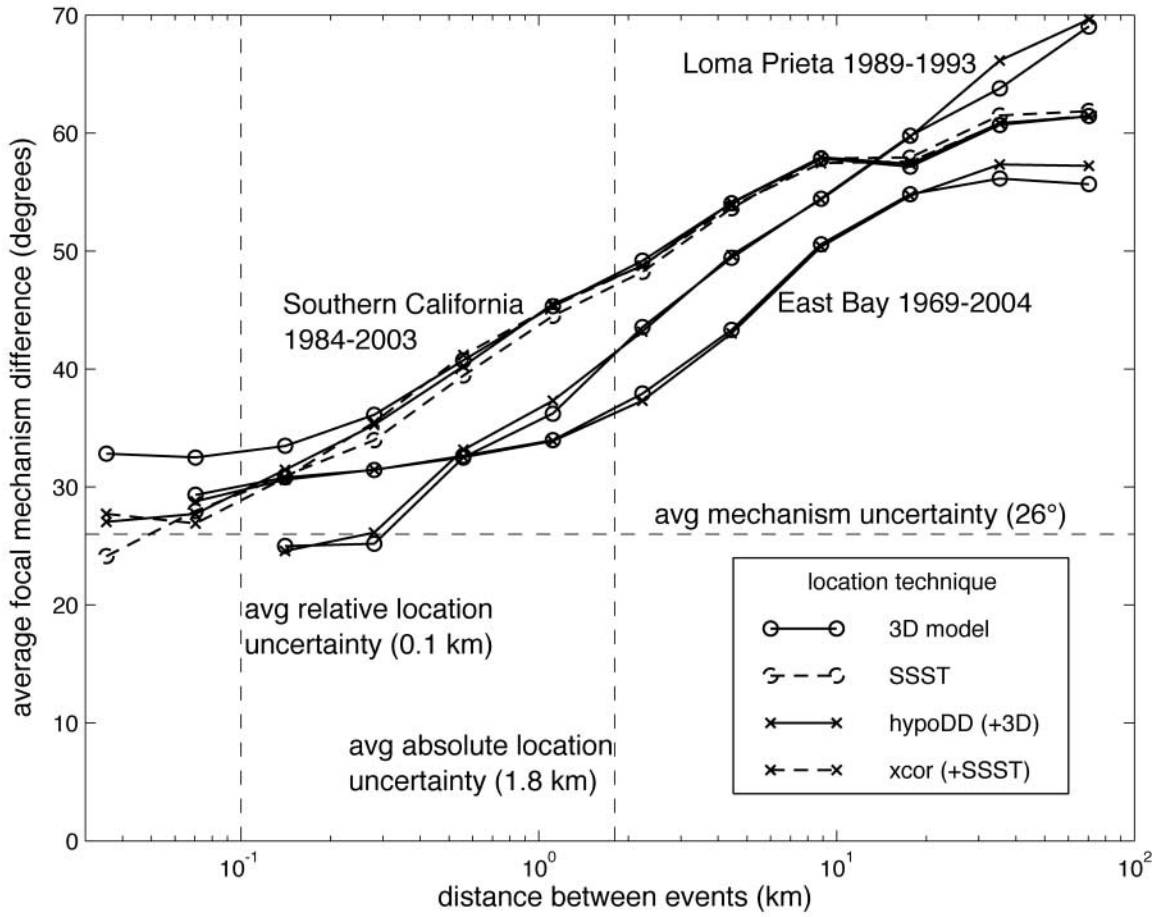

Figure 2. Mean focal-mechanism difference between pairs of earthquakes, as a function of their hypocentral distance. Hypocenteral distance and focal-mechanism difference, defined as the minimum rotation angle between the mechanisms, were found for all event pairs, and the mean focal-mechanism difference was determined for each distance bin. Hypocenteral distance was found by using relocations from 3D seismic-velocity models (Eberhart-Phillips and Michael, 1998; Hauksson, 2000; Hardebeck *et al.*, 2004), double-difference (hypoDD) relocations (Hauksson and Shearer, 2005), source-specific station term (SSST) relocations (Richards-Dinger and Shearer, 2000), and relative relocation of similar event clusters from cross-correlation (xcor) (Shearer *et al.*, 2005). The mean formal 1σ uncertainties for the absolute SSST locations (1.8 km), for the relative locations within event clusters (0.1 km), and for the focal mechanisms (26°) are indicated with dashed lines.

imum to another. If there are a few very different mechanisms (incorrect local minima) in an otherwise homogeneous dataset, the large difference angles associated with these events form the long tail of the distribution. The angular difference histograms for short interevent distances for the three California datasets show similar long tails (Fig. 5b–d), strongly suggesting that much of these tails are due to focal-mechanism measurement errors and not actual heterogeneity. A comparison with synthetics where the "correct" focal mechanisms vary up to 10° from a reference mechanism (Fig. 5b–d) shows that the long tails of the observed distributions are consistent with $\leq 10°$ variation in the true mechanisms.

The observed increase in heterogeneity with length scale is a general feature over the entire spatial extent of the southern California dataset and is not driven by any particular region. The shading of each spatial bin in Figure 6 shows the average focal-mechanism difference between each event in the bin and all events 0–0.1, 0.1–1, 1–10, and 10–100 km distant from that event. There is scatter in the average mechanism similarity, but this scatter is similar over the whole dataset. The average mechanism difference for all regions of southern California increases with distance.

I also investigate the similarity between temporally clustered events. This is complicated by the joint spatial-temporal clustering of earthquakes, because events that are closer in time may be more similar just because they are closer in space. A plot of average mechanism difference as a function of both space and time (Fig. 7) shows that the spatial pattern of decreased mechanism similarity with dis-

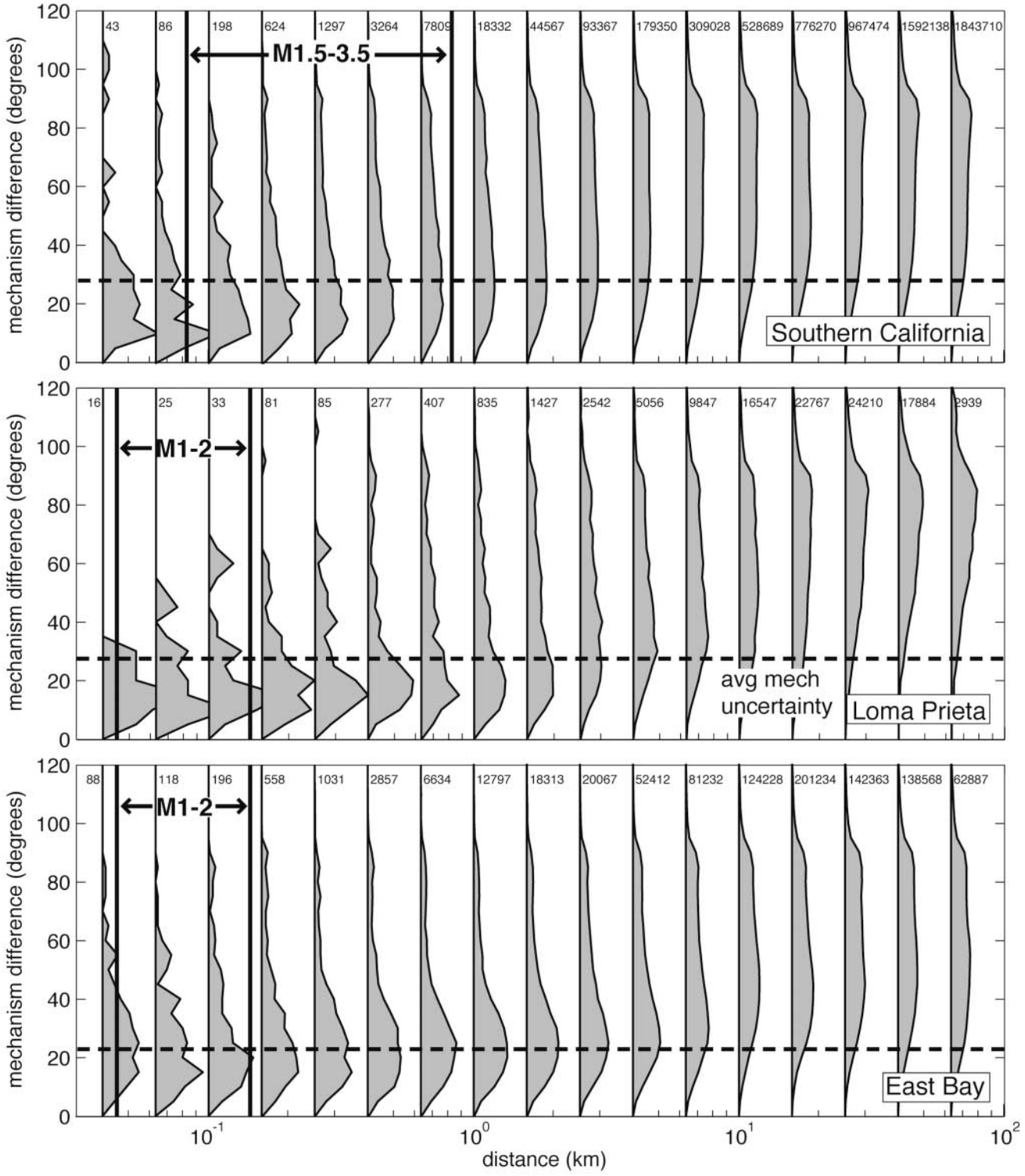

Figure 3. Distribution of focal-mechanism differences between pairs of earthquakes, as a function of the hypocentral distance. As in Figure 2, except that a histogram of the mechanism differences for each distance bin is shown, instead of the mean. The histograms are on their sides, with the difference axis vertical and the count axis horizontal. The small number at the top of each histogram indicates the number of event pairs in this bin, and the histogram is scaled by this number. Also shown are the average formal mechanism errors for each dataset (dashed horizontal lines), and the rupture length scales for the predominant earthquake magnitude range for each dataset, assuming circular faults with 3-MPa stress drop (solid vertical lines). Hypocentral distances were found using the hypoDD locations.

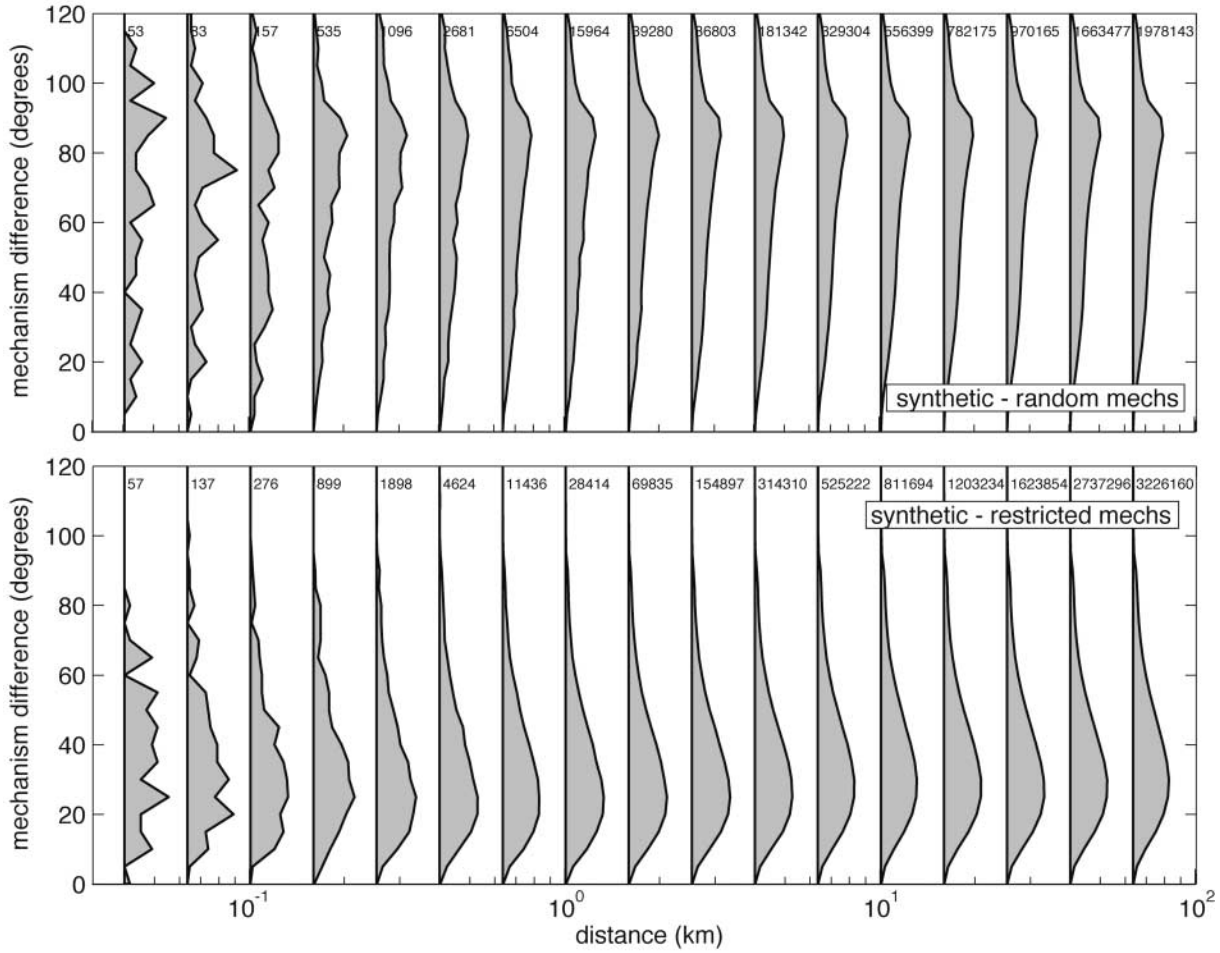

Figure 4. As in Figure 3, except for synthetic datasets. The source and station locations are the same as the real southern California dataset, with "correct" focal mechanisms assigned randomly either from the whole set of observed mechanisms (top) or from a restricted subset of similar mechanisms (bottom). Polarity values are assigned to stations assuming that Hauksson's (2000) 3D velocity model is the "true" velocity structure, and a set of 1D velocity models are used in the computation of the focal mechanisms, simulating the effects of unmodeled velocity structure. Measurement error is introduced by randomly reversing 10% of the synthetic polarity data, and adding a 30% error to synthetic *S*/*P* amplitude ratios. Focal mechanisms are computed just as they were for the real dataset, and high-quality solutions are selected using the same criteria.

tance persists over all timescales. Although the spatial pattern is stronger than the temporal pattern, there appears to be a small increase in mechanism similarity between events closer in time.

This analysis shows that active fault structures are quite homogeneous on very short length scales (<0.5–5 km), often identical to within the measurement uncertainty of ~25° (although the nodal plane ambiguity leaves open the possibility that some earthquakes are on orthogonal planes [e.g., Kilb and Rubin, 2002]). There is no need for any stress tensor or fault strength heterogeneity on these short length scales, the similar focal mechanisms can be explained by homogeneous stress and fault strength. However, the fault structures become more heterogeneous on larger (>10 km) length scales. I next examine the implications of the focal mechanism variability on ~10-km length scales for the degree of heterogeneity of stress and fault strength on these scales.

Stress and Fault Strength

The level of heterogeneity of earthquake focal mechanisms has direct implications for the stress in the crust and for the strength of faults, because highly heterogeneous focal mechanisms are inconsistent with the assumption of uniform stress and fault strength. Rivera and Kanamori (2002) found a variety of focal mechanisms for southern California earthquakes and concluded that the stress orientation or the fault

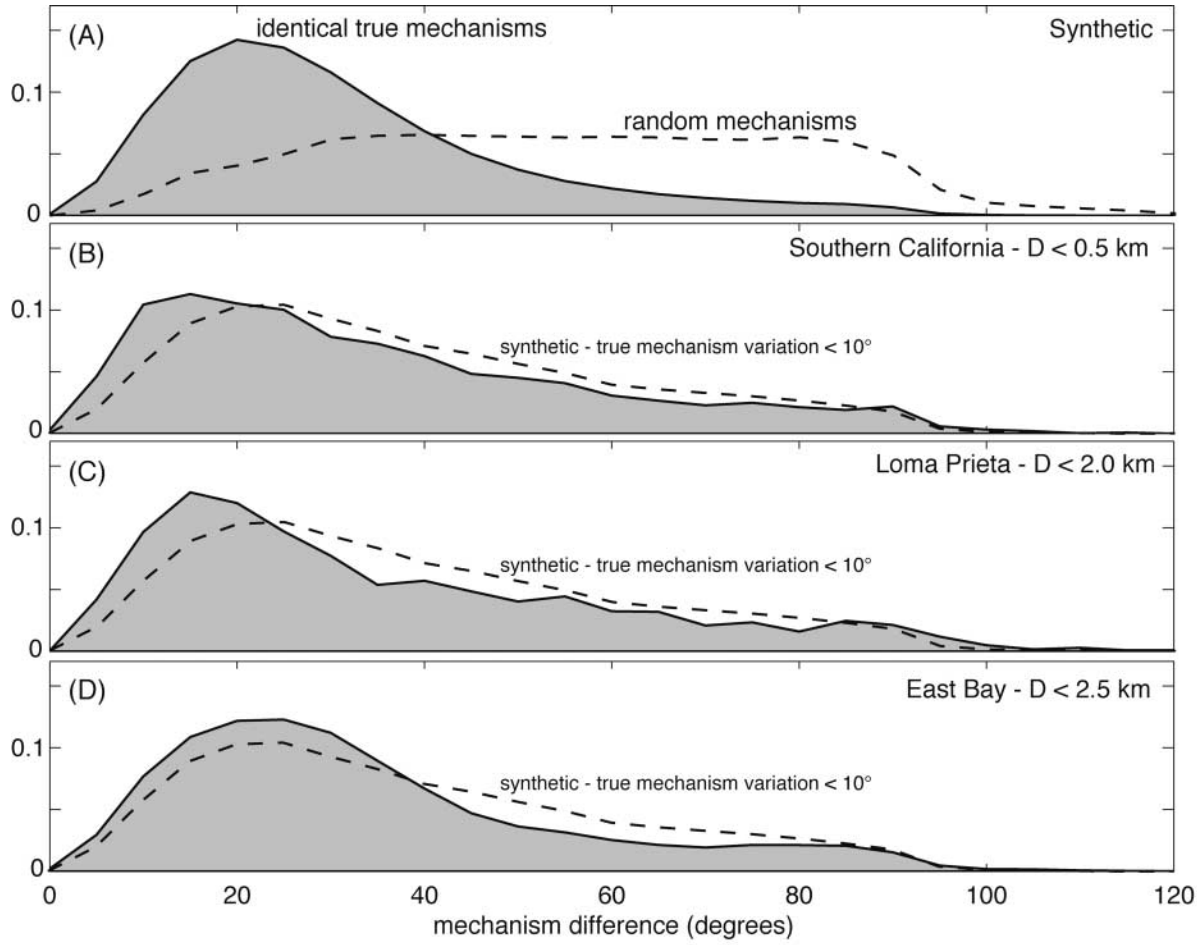

Figure 5. Distribution of angular focal-mechanism differences between pairs of earthquakes. (a) For synthetic datasets (as in Fig. 4), with the "correct" focal mechanisms all identical (shaded), and with random "correct" focal mechanisms (dashed). (b) For the observed Southern California dataset, for all event pairs less than 0.5 km apart (shaded), compared with synthetics with "correct" focal mechanisms with $<10°$ variation (dashed). (c) For the observed Loma Prieta dataset, for all event pairs less than 2 km apart (shaded), compared with synthetics with $<10°$ variation (dashed). (d) For the observed East Bay dataset, for all event pairs less than 2.5 km apart (shaded), compared with synthetics with $<10°$ variation (dashed).

strength, or both, must be very heterogeneous. They first assumed a constant stress tensor for all of southern California and projected the stress onto the fault plane of each earthquake. They then found the coefficient of friction, $\mu = \tau/\sigma_{\text{eff}}$, where τ is the shear stress and σ_{eff} is the effective normal stress, for each event. The distribution of μ was broad, indicating that if stress is constant, a wide range of fault frictional strengths is required. Next, they assumed constant fault strength and found for each earthquake the stress tensor in which the fault plane was optimally oriented for failure. They found stress tensors of many orientations, implying that if fault strength is constant, stress must be heterogeneous. They further hypothesized that reality may be somewhere in between these end members, with heterogeneity in both the stress field and fault strength. This has important implications for earthquake physics, as large stress or strength heterogeneities imply a wide range of fault behaviors in response to applied stress.

I perform a similar analysis on the new southern California focal-mechanism dataset. I find the best-fitting stress tensor for the entire southern California focal-mechanism dataset, using the technique of Michael (1984) ($\sigma_{\max}$ trending N11°E, σ_{med} vertical, $R = (\sigma_{\max} - \sigma_{\text{med}})/(\sigma_{\max} - \sigma_{\min}) = 0.37$). The stress inversion does not constrain absolute stress magnitudes, so the relative magnitude of the isostatic and deviatoric parts of the stress tensor must be imposed by choosing $\mu_{\max}$, the maximum $\mu = \tau/\sigma_{\text{eff}}$ over all plane orientations. I then project the full stress tensor (found from the orientations of the three principal axes, the stress ratio R, and the assumed value of $\mu_{\max}$) onto the fault plane of each earthquake (resolving the nodal plane ambiguity by using the plane with the greatest Coulomb stress, $\text{CS} = \tau +$

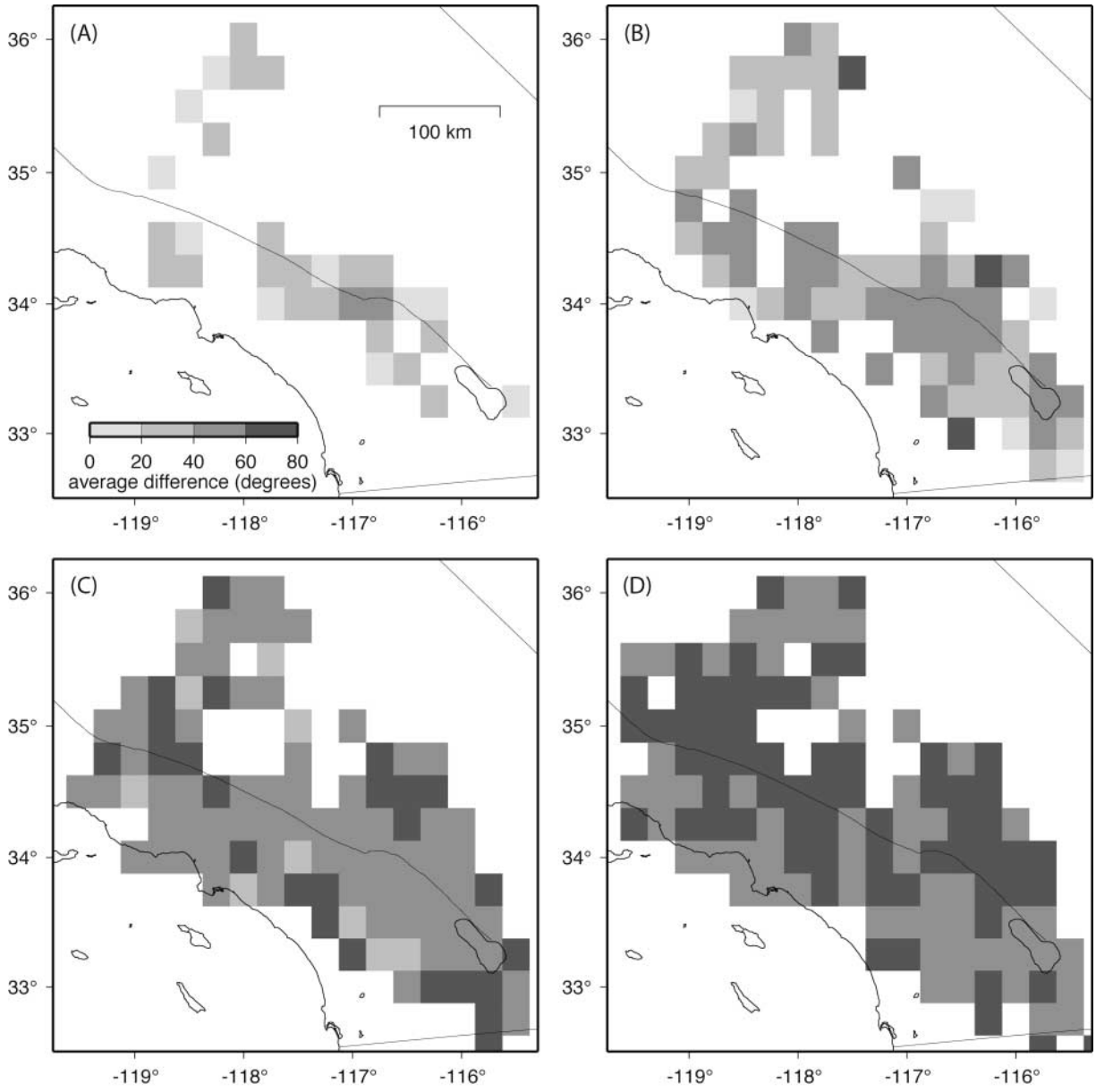

Figure 6. Maps of average mechanism differences for southern California earthquakes on a range of length scales. The shading of each 0.25° × 0.25° bin shows the average focal mechanism difference between each event in the bin and all events (a) 0–0.1 km distant, (b) 0.1–1 km distant, (c) 1–10 km distant, and (d) 10–100 km distant from that event. Bins containing no earthquakes within the given distance range from other events are shown in white. Coastlines and the surface trace of the San Andreas fault are shown as black lines.

$\mu_{max}\sigma_{eff}$), find $\mu = \tau/\sigma_{eff}$, and plot a histogram of the distribution of μ/μ_{max} (Fig. 8a). For a wide range of plausible values of μ_{max} (0.1–0.8), most earthquakes have $0.6 \leq \mu/\mu_{max} \leq 1.0$. This is a narrower distribution of values than found by Rivera and Kanamori (2002), presumably because I use a higher-quality dataset.

I then assume constant fault frictional strength, $\mu = \mu_{max}$, for each fault and find the stress tensor for which the fault is optimally oriented for failure. The orientations of the three stress axes follow from the fault orientation and μ, but the relative stress magnitude $R = (\sigma_{max} - \sigma_{med})/(\sigma_{max} - \sigma_{min})$ is not constrained. R is chosen to minimize the scaled tensor dot product between the deviatoric stress tensor and the best-fitting deviatoric stress tensor for the region, so as to not introduce any unnecessary apparent stress heterogeneity. I then plot histograms of the scaled tensor dot products between the optimally oriented deviatoric stress tensor for each event and the regional deviatoric stress tensor. For a

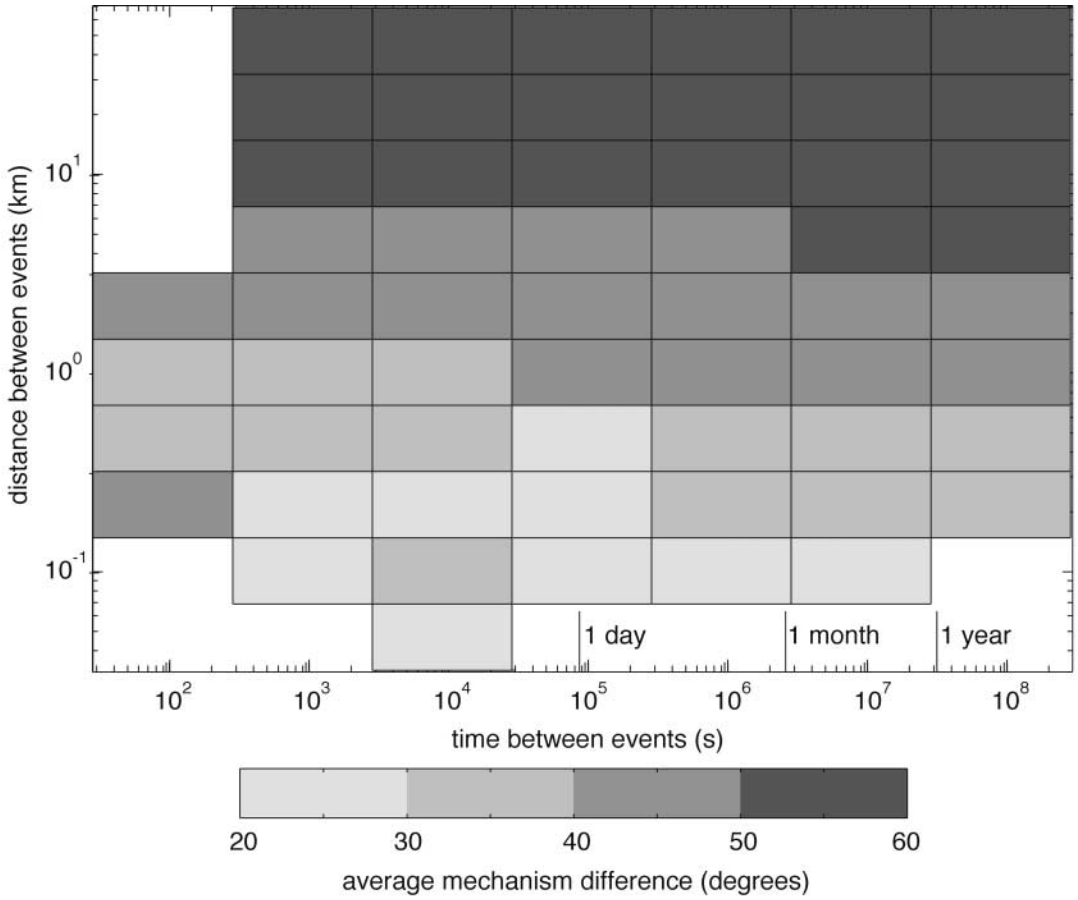

Figure 7. Spatial-temporal distribution of focal-mechanism differences. For every pair of events in the southern California dataset, the focal-mechanism difference was found, along with the spatial and temporal separation between the events. The average mechanism difference is shown for each spatial-temporal bin.

wide range of plausible values of μ_{max}, most dot products are between 0.7 and 1.0, where 1.0 indicates identical stress tensors (Fig. 8b). Rivera and Kanamori (2002) don't quantify stress heterogeneity in the same way, but this seems like a narrower distribution than implied by their results, again presumably due to fewer measurement errors in the focal mechanisms.

These analyses mix events from the entire southern California catalog, although we know that this region contains several tectonic provinces with different styles of faulting (e.g., Hutton *et al.*, 1991), which may have different stress states even if stress is locally homogeneous within each province. Differences between provinces may be responsible for some of the spread in the histograms in Figure 8a,b. To remove the large-scale changes in stress orientation across these different tectonic regimes, I use a smoothly varying stress orientation model (Becker *et al.*, 2004; Hardebeck and Michael, 2005) with stress variations on length scales of ~50 km (Fig. 9).

I repeat the exercise of projecting the full stress tensor onto each earthquake fault plane, but this time I use the stress tensor from the smoothly varying stress model at the location of the earthquake. The distribution of μ/μ_{max} is considerable more peaked, with $0.7 \leq \mu/\mu_{max} \leq 1.0$ for most earthquakes (Fig. 8c). Similarly, I fix $\mu = \mu_{max}$ for each fault, and find the difference between the optimally oriented stress tensor and the local stress from the smoothly varying stress model. This distribution is also considerably more peaked, with most tensor dot products between 0.8 and 1.0 (Fig. 8d). These results indicate that a considerable amount of the apparent stress or strength heterogeneity, in this dataset and presumably also in Rivera and Kanamori's (2002) dataset, comes from mixing events from the strike-slip, thrust, and normal faulting regimes of southern California. The southern California dataset requires only mild local variations of stress and/or strength (~30% in fault strength and/or a tensor dot product of 0.8, which is approximately equivalent to ~20° in stress orientation) on ~10-km length scales, in addition to the large-scale (~50 km) stress differences across the different tectonic regimes.

I also consider the effect of focal-mechanism uncertainty on the apparent variations in stress and fault strength. I repeat these exercises again, using the smoothly varying stress model, this time also searching over the 1σ confidence

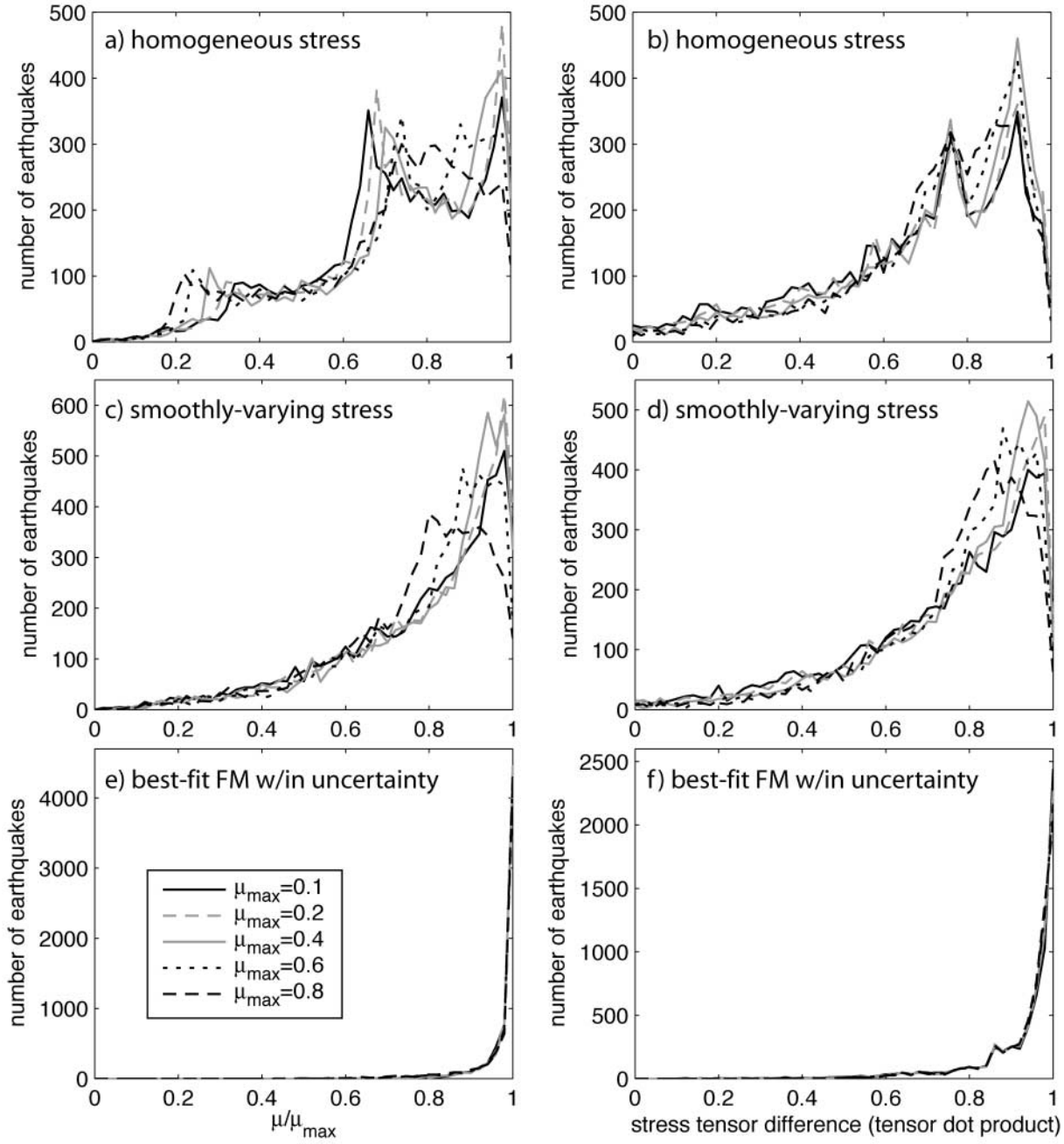

Figure 8. The distribution of fault strength (left) or stress tensor variations (right) implied by the southern California focal-mechanism dataset. To test the variation in fault frictional strength required by a homogeneous stress state, the shear stress and normal stress is resolved on the preferred fault plane of each earthquake and used to compute the coefficient of friction, μ. The left panels show histograms of the distribution of μ/μ_{max} for a range of values of μ_{max} (μ_{max} is related to the ratio of the isotropic and deviatoric parts of the stress tensor). To test the variation in stress state required by homogeneous fault strength, a stress tensor is found for each earthquake such that the preferred fault plane is optimally oriented for failure assuming friction coefficient μ_{max}. The right panels show histograms of the distribution of the scaled tensor dot product between the deviatoric stress tensor for each event and the best-fitting deviatoric stress tensor, for a range of values of μ_{max}. (a) and (b) assume a homogeneous stress field for all of southern California, found using the technique of Michael (1984). (c) and (d) use the smoothly varying stress field shown in Figure 9 (Hardebeck and Michael, 2005). (e) and (f) instead of using the preferred focal mechanism (FM), use the focal mechanism within the 1σ uncertainty that maximizes μ/μ_{max} or the tensor dot product.

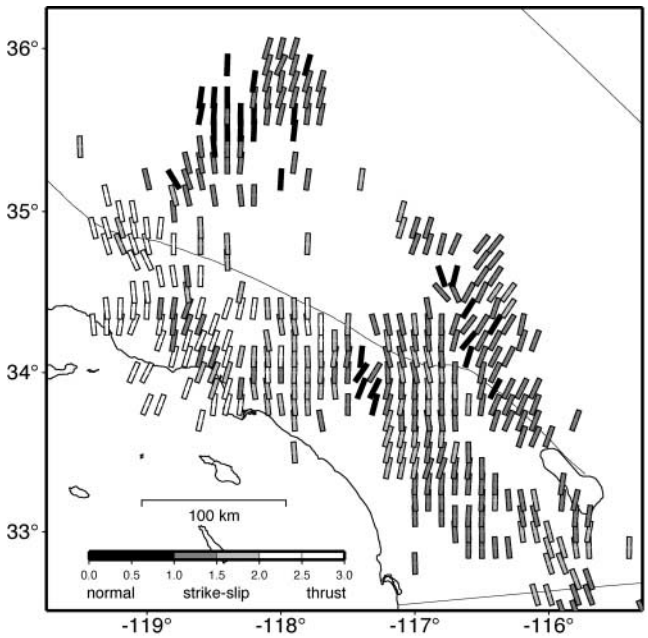

Figure 9. Smoothly varying stress field for southern California. The bar orientation shows the direction of the maximum horizontal stress axis, and the shading of the bar indicates the stress regime, following Simpson (1997). The stress orientations were found by simultaneously inverting the data for each grid point, while minimizing the difference between stress tensors at adjoining grid points, using the method of Hardebeck and Michael (2005).

region of each focal mechanism to find the mechanism that maximizes μ/μ_{max} or the tensor dot product. In this case, μ/μ_{max} and the dot product are ~1.0 for most events (Figs. 8e and 3f), and at most a ~15° variation in stress orientation and/or a ~10% variation in fault strength is required. Therefore, completely homogeneous local stress and fault strength cannot be ruled out, with the apparent variation coming entirely from focal-mechanism measurement errors. So stress and strength in the crust may be homogeneous on short to intermediate (less than a few tens of kilometers) length scales, and smoothly varying at longer length scales.

Discussion

The results presented previously can be used to characterize the degree of homogeneity or heterogeneity in the geometry of earthquake faulting, stress orientation, and fault strength on a range of length scales. On the longest length scales, the earthquake focal mechanisms are fit well by a smoothly varying stress field (Hardebeck and Michael, 2005) with stress-orientation variations on scales of ~50 km.

On intermediate length scales (>0.5–5 km and <50 km), earthquake fault planes are similar enough that they can be explained by a relatively homogeneous stress state and relatively homogeneous fault strength. If the focal mechanisms are taken to be exact, some variability is required in either the stress orientation or the fault strength, although not as large as the variability proposed by Rivera and Kanamori (2002). For example, most fault planes have a coefficient of friction within 30% of that of the optimally oriented plane. Measurement error in the focal mechanisms (estimated to be ~26° on average) may be responsible for much of the apparent variability in fault orientation. If the true focal mechanism of each event is assumed to be the mechanism within the 1σ confidence region that best fits the average local stress tensor, very little variation in stress orientation (<15°) or fault strength (<10%) is required. Therefore, nearly homogeneous stress and fault strength on these scales cannot be ruled out.

On the shortest length scales (<0.5–5 km), nearby earthquakes generally occur on fault planes of similar orientations, often with identical focal mechanisms to within the 1σ uncertainty. Repeating microearthquakes with identical seismograms (e.g., Nadeau *et al.*, 2004) support the idea that colocated events have identical sources. The mechanism similarity implies that in small volumes of crust, although faults and fractures of many orientations may or may not be present, only similarly oriented fault planes are active contemporaneously. Similarly, Barton *et al.* (1995) observed a wide variety of fracture orientations in three 1.7- to 3.5-km-deep boreholes, but only the favorably oriented fractures were hydraulically conductive suggesting recent activity. Focal mechanisms are highly similar even at distances greater than the earthquake dimension, for two of the three regions considered, implying the similarity is not due solely to the instability of cross-cutting faults. Clearly on these short length scales, no stress-orientation heterogeneity or fault-strength heterogeneity is required to explain the observed fault orientations.

Stress orientations inferred from borehole breakouts in the 3.5-km-deep Cajon Pass borehole and the 2.2-km-deep SAFOD pilot hole near the San Andreas fault in California vary significantly on length scales from ~1 m to ~1 km (Shamir and Zoback, 1992; Hickman and Zoback, 2004), in apparent contradiction with these results. However, it may be that stress heterogeneity is limited to these relatively shallow depths where the stress tensor has lower absolute magnitude and is more easily perturbed. At greater depths, where most of the small earthquakes used in this study occurred, higher lithostatic stress may inhibit perturbations. In the deep KTB borehole in Germany, the observed borehole breakout orientations at 3–7 km depth are more coherent (Brudy *et al.*, 1997), possibly reflecting more homogeneous stress at greater depth. Of course, the differences between these two boreholes may be due to regional characteristics instead.

It has been proposed (Smith and Heaton, 2004) that the background stress field is heterogeneous, but this background stress is not directly reflected in the orientations of small earthquakes. Earthquakes in this model occur in response to a homogeneous tectonic loading stress, and the fault planes that fail are more aligned with the tectonic load-

ing than the local background stress. In Smith and Heaton's (2004) simulations of this model with high levels of background stress heterogeneity, highly heterogeneous focal mechanisms are predicted. However, if smoothing is applied to the background stress, decreased mechanism similarity with interevent distance is predicted (D. Smith, personal comm., 2005), similar to the observations in Figures 2 and 3. Therefore, this model cannot be ruled out, as long as it includes smoothing to keep the stress relatively homogeneous on short length scales.

Some large earthquakes have been shown to locally increase stress heterogeneity (e.g., Michael *et al.*, 1990; Hauksson, 1994; Castillo and Zoback, 1995; Hardebeck and Hauksson, 2001). The focal mechanisms studied here include the aftershock sequence of the M_w 6.9 Loma Prieta earthquake, which is known for a particularly wide variety of aftershock orientations (e.g., Michael *et al.*, 1990; Beroza and Zoback, 1993; Kilb *et al.*, 1997). This variability is apparent in the high average mechanism differences for distant and medium-range (>2-km interevent distances) pairs of aftershocks (Fig. 2), equivalent to the length scales implicit in the previous studies. The aftershocks occurring along the mainshock rupture exhibit more mechanism variability at shorter length scales than the aftershock sequence as a whole, reflecting the roughness of the mainshock slip (Fig. 10). However, the focal mechanisms of very close (<0.5 km) aftershocks are everywhere quite similar. Either the mainshock slip may have been homogeneous at short length scales (<0.5 km), or whatever small-scale stress heterogeneity was produced by the mainshock may have been smoothed away quickly by afterslip or early aftershocks.

The similarity of nearby focal mechanisms is interpreted to imply that the strength of the faults, as measured by the coefficient of friction, is also similar. However, prior work has suggested that more mature faults with greater offset have lower coefficients of friction. For example, Parsons *et al.* (1999) compared the change in seismicity rate on different faults with the modeled static stress changes from nearby large earthquakes. They concluded that major faults are not as responsive to normal stress changes as minor faults, indicating a lower coefficient of friction for mature faults. Seismicity in southern California occurs primarily off of the major faults, so the histograms in Figure 8 reflect the strength variability of the minor faults. The strength of the San Andreas fault has been estimated from the angle that σ_{max} makes to the fault, and although the results are contro-

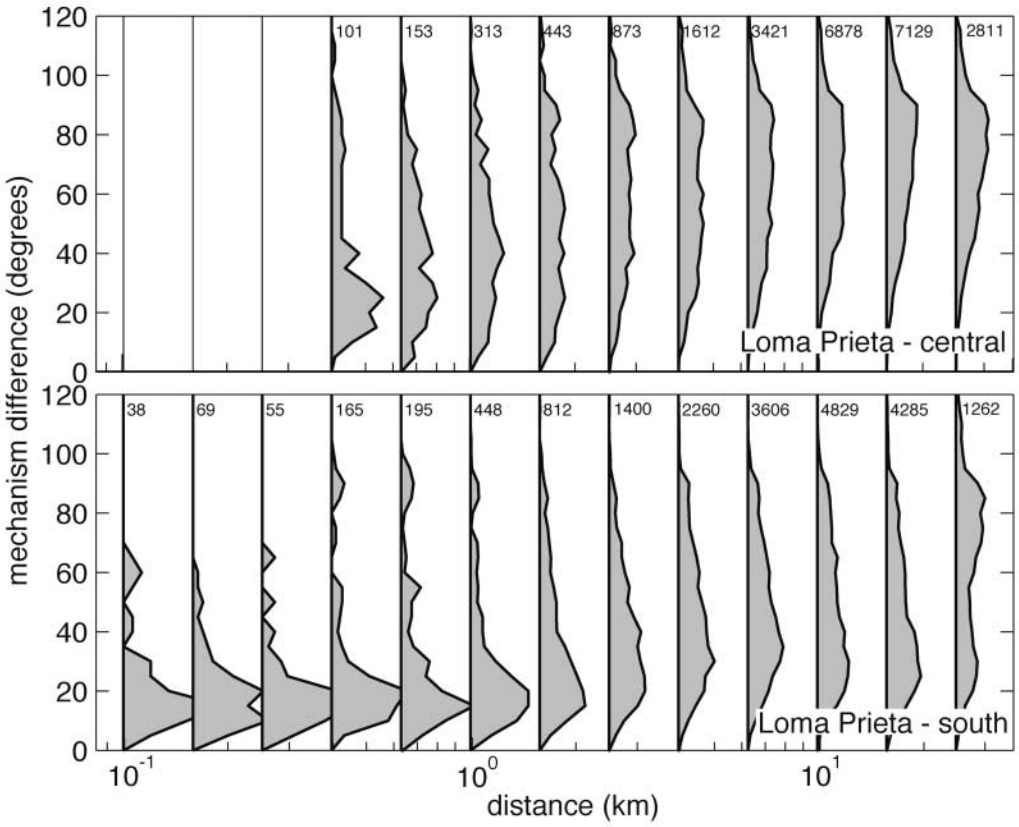

Figure 10. Distribution of focal-mechanism differences between pairs of earthquakes as a function of the hypocentral distance (as in Fig. 3), for two subsets of the Loma Prieta dataset. The "central" section contains aftershocks immediately along and above the mainshock rupture (as in Michael *et al.* [1990]), and the "south" section contains aftershocks occurring to the south of the mainshock rupture.

versial, it appears that the strength of the San Andreas fault is on the same order as the surrounding minor faults (e.g. Hardebeck and Michael, 2004).

Conclusions

The analysis of focal-mechanism data reveals that earthquake fault planes are more homogeneous than previously thought. Some of the decrease in variability comes from using higher-quality datasets, eliminating some of the measurement error that may increase the apparent fault-plane heterogeneity. This analysis also differs from previous work by more carefully considering the role of measurement error when comparing focal mechanisms and making inferences about the degree of heterogeneity in fault strength or in crustal stress orientation.

Focal mechanisms are most similar, often identical to within the 1σ uncertainty, on short length scales of $<$0.5–5 km, and on these scales no stress or strength heterogeneity is needed. On greater length scales, mechanisms become more diverse, but are usually consistent with only minor variability in fault strength ($<$30%) or stress orientation ($<20^\circ$), even if no mechanism uncertainty is considered. If each earthquake is assigned the optimal focal mechanism within its 1σ confidence region, very little heterogeneity in fault strength ($<$10%) or stress orientation ($<15^\circ$) is required to explain the distribution of fault planes, other than a smoothly varying stress field on length scales of $\sim$50 km.

If fault geometry, stress, and fault strength are generally homogeneous on $\sim$10-km length scales, this is encouraging for understanding earthquake physics. It may be possible to measure these parameters with enough precision to be useful in studying and modeling large earthquakes and the behavior of major faults.

Acknowledgments

I thank the Southern California Seismic Network (SCSN), the Northern California Seismic Network (NCSN), the Southern California Earthquake Data Center (SCEDC), and the Northern California Earthquake Data Center (NCEDC) for collecting and providing the earthquake first-motion data used to generate the focal mechanisms. I thank Peter Shearer and Egill Hauksson for running my *P*- and *S*-wave amplitude codes on their southern California waveform database. I thank Peter Shearer, Egill Hauksson, Guoqing Lin, and Keith Richards-Dinger for making their earthquake relocation datasets available on the SCEDC web site. I thank Andy Michael for helpful discussions, and for assisting me with his 3D velocity model for Loma Prieta. I am grateful to Andy Michael, Karen Felzer, Steven Jaume, and an anonymous reviewer for their helpful comments on the manuscript.

References

Barton, C. A., M. D. Zoback, and D. Moos (1995). Fluid flow along potentially active faults in crystalline rock, *Geology* **23,** 683–686.

Becker, T. W., J. L. Hardebeck, and G. Anderson (2004). Constraints on fault slip rates of the southern California plate boundary from GPS velocity and stress inversions, *Geophys. J. Int.* doi 10.1111/j.1365-246X.2004.02528.x.

Beroza, G. C., and M. D. Zoback (1993). Mechanism diversity of the Loma Prieta aftershocks and the mechanics of mainshock-aftershock interaction, *Science* **259,** 210–213.

Brudy, M., M. D. Zoback, K. Fuchs, F. Rummel, and J. Baumgärtner (1997). Estimation of the complete stress tensor to 8 km depth in the KTB scientific drill holes: implications for crustal strength, *J. Geophys. Res.* **102,** 18,453–18,475.

Castillo, D. A., and M. D. Zoback (1995). Systematic stress variations in the southern San Joaquin Valley and along the White Wolf fault: implications for the rupture mechanics of the 1952 Ms 7.8 Kern County earthquake and contemporary seismicity, *J. Geophys. Res.* **100,** 6249–6264.

Eberhart-Phillips, D., and A. J. Michael (1998). Seismotectonics of the Loma Prieta, California, region determined from three-dimensional Vp, Vp/Vs, and seismicity, *J. Geophys. Res.* **103,** 21,099–21,120.

Hardebeck, J. L., and E. Hauksson (2001). Crustal stress field in southern California and its implications for fault mechanics, *J. Geophys. Res.* **106,** 21,859–21,882.

Hardebeck, J. L., and A. J. Michael (2004). Stress orientations at intermediate angles to the San Andreas Fault, California, *J. Geophys. Res.* **109,** B11303, doi 10.1029/2004JB003239.

Hardebeck, J. L., and A. J. Michael (2005). Damped regional-scale stress inversions: methodology and examples for Southern California and the Coalinga aftershock sequence, *J. Geophys. Res.* (in press).

Hardebeck, J. L., and P. M. Shearer (2002). A new method for determining first-motion focal mechanisms, *Bull. Seism. Soc. Am.* **92,** 2264–2276.

Hardebeck, J. L., and P. M. Shearer (2003). Using S/P amplitude ratios to constrain the focal mechanisms of small earthquakes, *Bull. Seism. Soc. Am.* **93,** 2434–2444.

Hardebeck, J. L., A. J. Michael, and T. M. Brocher (2004). Seismic velocity structure and seismotectonics of the Hayward Fault System, East San Francisco Bay, California (abstract), *EOS Trans. AGU* **85,** no. 47 (Fall Meeting Suppl.), S34A-05.

Hauksson, E. (1994). State of stress from focal mechanisms before and after the 1992 Landers Earthquake sequence, *Bull. Seism. Soc. Am.* **84,** 917–934.

Hauksson, E. (2000). Crustal structure and seismicity distribution adjacent to the Pacific and North America plate boundary in Southern California, *J. Geophys. Res.* **105,** 13,875–13,903.

Hauksson, E., and P. Shearer (2005). Southern California hypocenter relocation with waveform cross-correlation. Part 1. Results using the double-difference method, *Bull. Seism. Soc. Am.* **95,** 896–903.

Hickman, S., and M. Zoback (2004). Stress orientation and magnitudes in the SAFOD pilot hole, *Geophys. Res. Lett.* **31,** L15S12, doi 10.1029/2004GL020043.

Hutton, L. K., L. M. Jones, E. Hauksson, and D. D. Given (1991). Seismotectonics of southern California, in *Neotectonics of North America: Boulder, Colorado*, D. B. Slemmons, et al. (Editors), Geol. Soc. Am. Decade Map, Vol. 1.

Kilb, D., and A. M. Rubin (2002). Implications of diverse fault orientations imaged in relocated aftershocks of the Mount Lewis, ML 5.7, California, earthquake, *J. Geophys. Res.* **107,** 2294, doi 10.1029/2001JB000149.

Kilb, D., M. A. Ellis, J. Gomberg, and S. D. Davis (1997). On the origin of diverse aftershock mechanisms following the 1989 Loma Prieta earthquake, *Geophys. J. Int.* **128,** 557–570.

Michael, A. J. (1984). Determination of stress from slip data; faults and folds, *J. Geophys. Res.* **89,** 11,517–11,526.

Michael, A. J., W. L. Ellsworth, and D. H. Oppenheimer (1990). Coseismic stress changes induced by the 1989 Loma Prieta, California earthquake, *Geophys. Res. Lett.* **17,** 1441–1444.

Nadeau, R. M., A. Michelini, R. A. Uhrhammer, D. Dolenc, and T. V. McEvilly (2004). Detailed kinematics, structure and recurrence of micro-seismicity in the SAFOD target region, *Geophys. Res. Lett.* **31,** doi 10.1029/2003GL019409.

Parsons, T., R. S. Stein, R. W. Simpson, and P. A. Reasenberg (1999). Stress sensitivity of fault seismicity: a comparison limited-offset

oblique and major strike-slip faults, *J. Geophys. Res.* **104,** 20,183–20,202.

Richards-Dinger, K., and P. Shearer (2000). Earthquake locations in southern California obtained using source-specific station terms, *J. Geophys. Res.* **105,** 10,939–10,960.

Rivera, L., and H. Kanamori (2002). Spatial heterogeneity of tectonic stress and friction in the crust, *Geophys. Res. Lett.* **29,** 1088, doi 10.1029/2001GL013803.

Shamir, G., and M. D. Zoback (1992). Stress orientation profile to 3.5 km depth near the San Andreas fault at Cajon Pass, California, *J. Geophys. Res.* **97,** 5059–5080.

Shearer, P., E. Hauksson, and G. Lin (2005). Southern California hypocenter relocation with waveform cross-correlation. Part 2: Results using source-specific station terms and cluster analysis, *Bull. Seism. Soc. Am.* **95,** 904–915.

Simpson, R. W. (1997). Quantifying Anderson's fault types, *J. Geophys. Res.* **102,** 17,909–17,919.

Smith, D. E., and T. H. Heaton (2004). Interpreting focal mechanisms in a heterogeneous stress field, *Seism. Res. Lett.* **75,** 279.

Waldhauser, F., and W. L. Ellsworth (2000). A double-difference earthquake location algorithm: method and application to the northern Hayward Fault, California, *Bull. Seism. Soc. Am.* **90,** 1353–1368.

U.S. Geological Survey
345 Middlefield Road, MS 977
Menlo Park, California 94025
jhardebeck@usgs.gov

Manuscript received 15 December 2005.